Clays and Clay Minerals, Vol. 66, No. 1, 86–95, 2018.

LOW-FREQUENCY ELECTRICAL CONDUCTIVITY OF AQUEOUS KAOLINITE SUSPENSIONS II: COUNTERION EFFECTS AND ESTIMATING STERN LAYER MOBILITIES OF COUNTERIONS

CHRISTIAN WEBER[1,*], MATTHIAS HALISCH[2], AND HELGE STANJEK[1]

[1] Clay and Interface Mineralogy, RWTH Aachen University, Bunsenstrasse 8, 52072 Aachen, Germany
[2] Leibniz Institute for Applied Geophysics, Dept. 5 Petrophysics and Borehole Geophysics, Stilleweg 2, 30655 Hannover, Germany

Abstract—The electrical state of the interface between a kaolinite-dominated clay sample and aqueous electrolyte solutions was characterized using low-frequency conductance measurements. From these measurements, the ζ-potential and surface conductivity contributions from the diffuse and non-diffuse parts of the electrical double layer were obtained. The suspensions were studied as a function of volume fraction, electrolyte concentration, and electrolyte type (LiCl, NaCl, KCl, CsCl, $CaCl_2$, $SrCl_2$, and $BaCl_2$). Interpretation in terms of the surface conductance revealed that a substantial part of the surface conductivity originates in the inner part of the double layer. Electrokinetic potentials and related diffuse double layer properties are highly dependent on the nature of monovalent counterions, whereas divalent counterions do not show such clear dependencies. Further presented was a simple way to estimate the order of magnitude of counterion mobilities in the inner part of the electrical double layer. All counterions were shown to have a substantial mobility in the inner part of the double layer. Finally, we suggest that the apparent ion-specific effects observed in the diffuse part of the double layer are at least in part related to the finite size of the counterions. Our findings are relevant to scenarios where fluid flow in porous media is accompanied by charged species transport, *e.g.*, in electro-osmotic remediation, spectral-induced polarization, or permeability measurements.

Key Words—Kaolinite, Spectral-induced Polarization, Stern Layer Mobility, Surface Charge Density, Surface Conductance, Zeta Potential.

INTRODUCTION

Surface charging and electrokinetic phenomena are a classical topic in clay and colloid science, because the formation of electrical double layers and the resulting distribution of ions has an impact in a wide range of situations. Nowadays, these phenomena have practical applications, such as soil remediation by electroosmotic flow (*e.g.*, Dzenitis, 1997), interpretation of spectral induced polarization (SIP) data (*e.g.*, Weller and Slater, 2015), or membrane filtration (*e.g.*, Labbez *et al.*, 2001).

Despite ample experimental data, however, a general and consistent interpretation of electrokinetic data, especially for clay minerals, is still lacking for various reasons: clay minerals have a non-spherical morphology, have pH-dependent and non-homogeneous charge distributions, may form aggregates, and are seldom in a pure state. What is less clear, however, is which of these factors are crucial for the interpretation of an experiment and which are less important.

Described in a previous article (Weber and Stanjek, 2017) was how to interpret low-frequency conductance measurements with internal consistency and how to derive electrokinetic (ζ) potentials, surface conductance, and counterion mobilities in the Stern layer.

In agreement with previous electrokinetic studies of clay suspensions (O'Brien and Rowlands, 1993; Rowlands and O'Brien, 1995; Rasmussen *et al.*, 1997; Chassagne *et al.*, 2009), a substantial fraction of surface conductance originated in the inner part of the double layer. In these studies, the authors were not able to quantify surface conductivity in the inner part of the double layer and estimates about the distribution of mobile charges within the double layer were not possible. Such information is not only interesting from an academic point of view, but is also vital for practical purposes.

A particular example are SIP measurements (*i.e.* 'low frequency range' impedance spectroscopy that is typically performed from 1 mHz to 1 kHz), which are used in many different ways to characterize porous media, especially sedimentary rocks and soils (Revil and Florsch, 2010; Revil, 2014; Weller *et al.*, 2015; Kruschwitz *et al.*, 2016; Weller *et al.*, 2016). Recent theoretical developments emphasize the links between interactions in the matrix-fluid-system and within the electrical double layer and correlations with petrophysical parameters, such as specific surface area, permeability, and the distribution of pore radii. A variety of polarization models, either grain based or pore based,

* E-mail address of corresponding author:
chris.weber@chemie.tu-freiberg.de
Current address: Institute for Physical Chemistry, Technical University Bergakademie Freiberg, 09599 Freiberg, Germany
DOI: 10.1346/CCMN.2018.064087

have been developed over the past years to describe the polarization effects in sedimentary rocks (*e.g.*, Scott and Barker, 2005; Tarasov and Titov, 2007; Kruschwitz *et al.*, 2010; Revil, 2012; Weller and Slater, 2015). Akin to the electrokinetic literature, most of these models distinguish between a purely diffuse part of the double layer and a Stern layer. In contrast to the inner part of the double layer, much theoretical and experimental information is available about the diffuse part. While the latter is entirely characterized by the ζ-potential, which is directly proportional to the charge density of the diffuse layer, the electrokinetic characterization of the inner part of the double layer relies on a determination of the surface conductivity in this region. This quantity can be expressed as (Lyklema, 1995):

$$K_2^{\sigma^i} = \sigma_2^i \cdot u_2^i \quad (1)$$

where $K_2^{\sigma^i}$ is the surface conductivity of the inner part of the double layer, σ_2^i is the charge density in this region, and u_2^i is the corresponding counterion mobility. Note that the subscript 2 indicates that only counterions are considered. This is an approximation that has been checked experimentally for similar systems (Weber and Stanjek, 2017). Equation 1 indicates that, apart from counterion adsorption in the inner part of the double layer, the ions need a certain mobility in order to produce inner layer surface conductance.

Based on the geophysical literature, neither the mobilities in the inner part of the double layer nor the corresponding charge densities have been sufficiently investigated in relevant systems. This hampers an understanding of the impact of these properties on low-frequency polarization effects in porous media. A specific example is found in discussions about the ionic mobilities within the Stern layer in clay-bearing systems, where surface complexation models predict a drastically reduced (by a factor of about 300) counterion mobility (Revil, 2012, 2014; Weller *et al.*, 2013).

The objective of the present contribution was to present low-frequency conductivity experiments on a kaolinite-dominated clay sample and to interpret the results with regard to ζ-potentials and the concentration dependence of inner- and diffuse-layer surface conductance values for different counterions (Li^+, Na^+, K^+, Cs^+, Ca^{2+}, Ba^{2+}, and Sr^{2+}). Furthermore, a simple way is presented to estimate the order of magnitude of the counterion mobility in the Stern layer, and thus provide valuable data to test the theoretical models mentioned in the previous paragraphs.

MATERIALS AND METHODS

A kaolinite-dominated clay sample from Horni Briza (Czech Republic) that contained 0.76 g/g kaolinite, 0.21 g/g illite/muscovite, and 0.03 g/g quartz was examined in the present study (Weber *et al.*, 2014). The kaolinitic material was exposed at least three times to >3 M LiCl, NaCl, KCl, or CsCl and to >1 M $CaCl_2$, $BaCl_2$, or $SrCl_2$ solutions, respectively. The samples were washed with deionized water during pressure filtration until the water reached an electrical conductivity of <2 μS/cm and then freeze-dried.

Electrical conductivities were measured at 25.0ºC in the same manner and with the identical equipment as described in Weber and Stanjek (2017). Aspect ratios of the kaolinitic samples were determined conductometrically at 5ºC (Weber and Stanjek, 2017) in a 100 mM $CaCl_2$ solution and the particle size distributions were assessed using acoustic spectroscopy and laser scattering as described in Weber *et al.* (2014). The suspension pHs ranged between 6 and 7 and depended slightly on the electrolyte type and concentration.

Nitrogen adsorption and desorption isotherms were recorded using a Micromeritics Gemini VII (Micromeritics Instrument Corporation, Norcross, Georgia, USA) at 77 K. The samples were outgassed in vacuum (p = 2.6 kPa) at 130ºC for 12 h. The BET (Brunauer *et al.*, 1938) surface areas were calculated following the recommendations of Rouquerol *et al.* (1994) and yielded a specific surface area of 15 m^2/g.

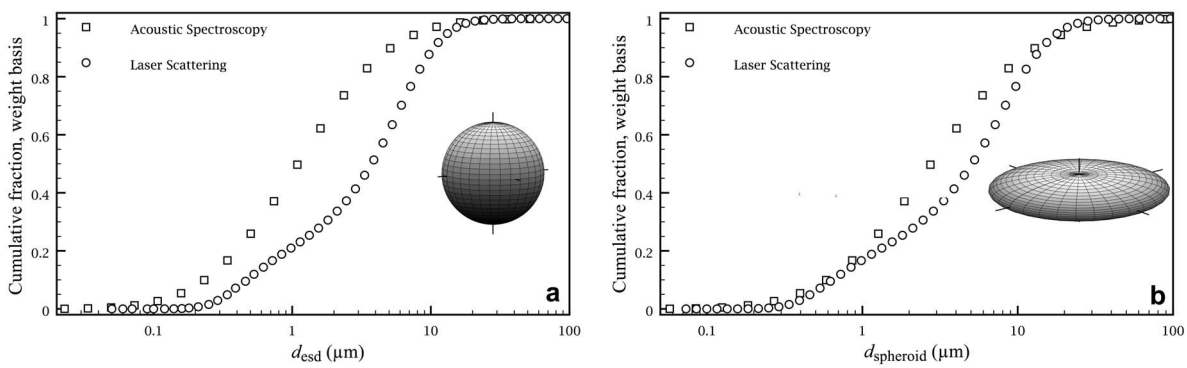

Figure 1. Cumulative particle size distributions from acoustic spectroscopy and laser scattering: (a) equivalent spherical diameters, (b) recalculated major diameters of oblate spheroids using the conductometrically determined aspect ratio (n = 1/24).

https://doi.org/10.1346/CCMN.2018.064087 Published online by Cambridge University Press

RESULTS AND INTERPRETATION

The particle size distributions determined by acoustic spectroscopy and by laser scattering (Figure 1a) were reproduced from Weber *et al.* (2014). The corresponding diameters of oblate spheroids (Figure 1b) were calculated with the aspect ratio determined conductometrically (n = 1/24) using the appropriate relationships presented in Jennings and Parslow (1988). The agreement between the two methods was improved when the

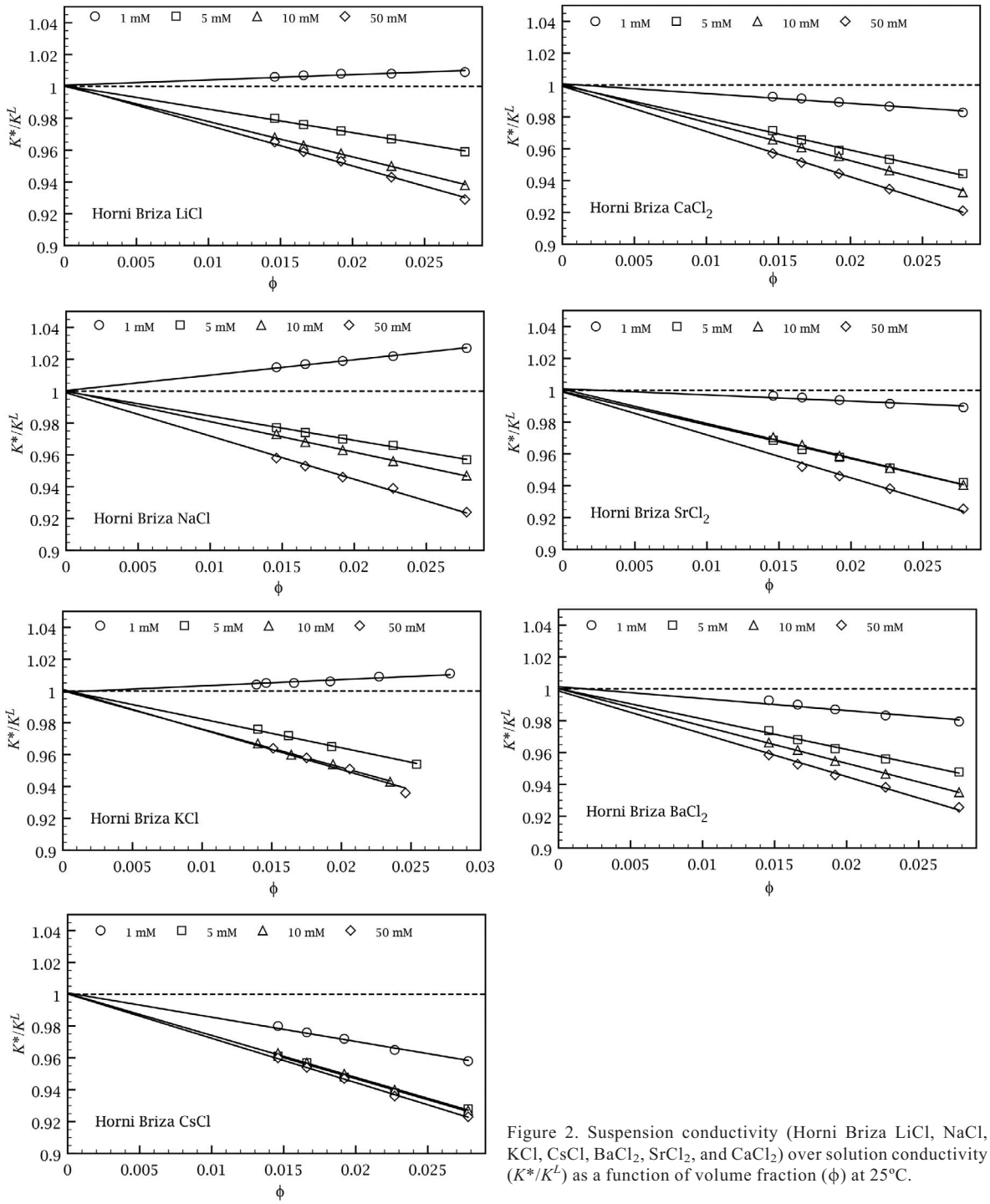

Figure 2. Suspension conductivity (Horni Briza LiCl, NaCl, KCl, CsCl, $BaCl_2$, $SrCl_2$, and $CaCl_2$) over solution conductivity (K^*/K^L) as a function of volume fraction (ϕ) at 25ºC.

https://doi.org/10.1346/CCMN.2018.064087 Published online by Cambridge University Press

particles were treated as oblate spheroids, but was not entirely satisfactory. This was partially because the actual distribution is bimodal, whereas the data evaluation scheme used to evaluate the acoustic spectroscopy data assumes log-normal distributions (more detail provided in Weber *et al.*, 2014). Also, the possibility that different size fractions have different aspect ratios (see Slepetys and Cleland, 1993) cannot be excluded.

Apart from these uncertainties, the other phases, especially illite/muscovite, may contribute to the bimodal character of the particle size distribution. Illite/muscovite may have a different aspect ratio than the dominant kaolinite phase. Because conductivity measurements performed here can only yield an average value of the quantity of interest, delineating the specific influence of accompanying phases using such macroscopic measurements is not possible. Anticipating the discussion about electrokinetic potentials and surface conductance, the impact of mineralogical impurities on electric surface parameters cannot be estimated for the same reasons outlined above. A reliable estimate of such effects would require very careful study of the pure components and defined mixtures. The principal behavior of the present sample is, however, similar to what was observed by Weber and Stanjek (2017), where a kaolinite with a different mineralogical composition was studied.

For the remainder of this article, the d_{50} of the laser scattering experiments, which is defined as the cumulative distribution median, will be taken as a guide. From this value, the major axis radius was calculated as a = 3.6 μm and the dimension of the minor half axis as b = 0.15 μm. Plots of the suspension conductivity/solution conductivity (K^*/K^L) ratio as a function of volume fraction ϕ (Figure 2) reveal that the various counterions behave quite differently from each other. Isoconductive points (K^*/K^L = 1) were observed for Li^+, Na^+, and K^+, but not for Cs^+ or the divalent cations. These observations give a first hint towards a certain ion specificity.

The $K^*/K^L(\phi)$ relationships were evaluated with the aid of O'Brien and Ward's theory, which is valid for randomly oriented particles with κl>>1. With the particle dimensions quoted above, κb ≈ 16−110 can be calculated for monovalent electrolytes and κb ≈ 27−191 for divalent electrolytes (the corresponding products for κa are a factor of 24 higher). For two species electrolytes, the relevant equation is (O'Brien and Ward, 1988):

$$\frac{K^*}{K^L} = 1 - \phi[f^0(0) + 2f^1(0)] - \frac{\phi D_2 z_2^2 n_z^\infty}{\sum_{j=1}^{N} D_j z_j^2 n_j^\infty} [f^0(Du_2) - f^0(0) + 2\{f^1(Du_2) - f^1(0)\}] \quad (2)$$

where D_2 is the counterion diffusion coefficient (subscript 2); z_2, the charge; n_2^∞, the number density [1/m^3] in the bulk solution; Du_2, the counterion Dukhin number; and the sum over j includes all solution species. The functional relationships for the f-functions of the oblate spheroids are collected in the Appendix of Weber and Stanjek (2017). Note that these functions depend only on the aspect ratio and the Dukhin number. Because the aspect ratio was determined independently, equation 2 can be solved explicitly for Du_2. The resulting Dukhin numbers showed the very same behavior that was already observed in Weber and Stanjek (2017) (see Figure 3). Du_2 is linear for inverse counterion conductivity $1/K_2^L$ and Du_2 is finite as $\frac{1}{K_2^L} \to 0$. This dependence was interpreted in terms of:

$$Du_2 = \frac{1}{K_2^L \cdot l} K_2^{\sigma^d} + Du_2^i \quad (3)$$

where l is a characteristic length scale of the particles, K_2^L is the conductivity contributed by the bulk counterions, $K_2^{\sigma^d}$ is the contribution of the diffuse layer to the surface conductivity, and Du_2^i is the Dukhin number of the inner part of the double layer. From equation 3, the slopes of the curves in Figure 3 are proportional to $K_2^{\sigma^d}$ and the intercepts are given by Du_2^i. For monovalent

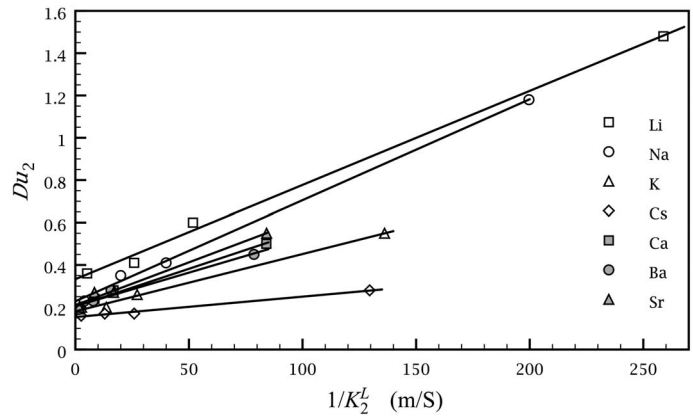

Figure 3. Du_2 as a function of inverse counterion conductivity at 25ºC.

https://doi.org/10.1346/CCMN.2018.064087 Published online by Cambridge University Press

counterions, both the slopes and intercepts are counterion-specific. The slopes decrease in the order $Li^+ \approx Na^+ > K^+ > Cs^+$ and the intercepts decrease in the order $Li^+ > Na^+ > K^+ > Cs^+$. Such pronounced slope and intercept variabilities, respectively, were not observed for divalent counterions. While the slope was somewhat higher for Sr^{2+}, the values for Ca^{2+} and Ba^{2+} were indistinguishable and the intercepts were identical for all three divalent counterions.

To calculate absolute surface conductivity and ζ-potential values, the characteristic length scale of the particles must be known. One option used to decide which is the relevant axis is to relate the surface conductivity to the independently measured surface charge density: (see Löbbus *et al.* (2000) and Weber and Stanjek (2017) for details)

$$K_2^\sigma = -u_2^i\sigma_2^0 + [(1+\frac{3m_2}{z_2^2})u_2^\infty - u_2^i]\sigma_2^d \qquad (4)$$

where K_2^σ is the surface conductivity calculated from $Du_2 = K_2^\sigma/(K_2{}^L \cdot l)$, u_2^∞ is the bulk ionic mobility, u_2^i is the corresponding ionic mobility value in the inner part of the double layer, σ_2^0 is the surface charge density due to the counterions, σ_2^d is the diffuse-layer charge density due to the counterions, and m_2 denotes the counterion ionic drag coefficient:

$$m_2 = \left(\frac{RT}{F}\right)^2 \frac{2\varepsilon\varepsilon_0}{3\eta D_2} \qquad (5)$$

where ε_0 is the permittivity of free space, ε is the relative dielectric constant of the solvent, and η is the viscosity.

Due to the relatively high aspect ratio, which translates into absolute surface conductivity values, $u_2{}^i$ is rather sensitive to the choice of characteristic length. Surface charge densities were determined for the CsCl sample (Figure 4) using ion chromatography (see Weber and Stanjek, 2017, for experimental details). For the surface conductivity values, $l = b = 0.15$ μm was used as the characteristic length scale. The inner layer to bulk mobility ratio was $u_{Cs}^i/u_{Cs}^\infty = 0.6 \pm 0.03$. If the major half-axis dimension had been used as the characteristic length, the mobility ratio would be around 14, which is far too high. Further support for the choice of $l = b$ stems from a comparison between (1) the diffuse-layer charge density calculated from the regression analysis intercept (σ_2^d (*reg*)) and (2) the diffuse-layer charge density computed from the ζ-potentials (σ_2^d (ζ)). From these calculations, we found that σ_2^d (*reg*) = 0.1 ± 0.2 μC/cm^2 and σ_2^d (ζ) = 0.12 ± 0.01 μC/cm^2. Although the particle size distributions do not match perfectly after correction for the particle shape, the reasonable value for the inner layer mobility, and the correspondence between the diffuse layer charge densities suggests that the choice of characteristic length was reasonable.

After deciding on the characteristic length value, the ζ potentials can be calculated from Du_2 by inverting

$$Du_2 = \frac{2}{K_2^L l}\frac{F^2 z_2^2 c^\infty}{RT\kappa} \left[D_2(e^{-z_2 y^{ek}/2} - 1)(1+\frac{3m_2}{z_2^2})\right] \cdot (1+\frac{K_2^{\sigma^i}}{K_2^{\sigma^d}}) \qquad (6)$$

which is valid for symmetrical electrolytes. For 2-1 electrolytes, such as $BaCl_2$, the relevant relation is (see Appendix of Weber and Stanjek, 2017):

$$Du_2 = \frac{12}{K_2^L l}\frac{F^2 c^\infty}{RT\kappa} \left[D_2\frac{e^{-y^{ek}/2}\sqrt{e^{-y^{ek}}+2} - \sqrt{3}}{\sqrt{3}}(1+\frac{3m_2}{z_2^2})\right](1+\frac{K_2^{\sigma^i}}{K_2^{\sigma^d}}) \qquad (7)$$

Because K_2^σ and $K_2^{\sigma^d}$ are known from the Dukhin number and from the respective straight line slopes in Figure 3, $K_2^{\sigma^i}$ can be obtained as $K_2^{\sigma^i} = K_2^\sigma - K_2^{\sigma^d}$. With

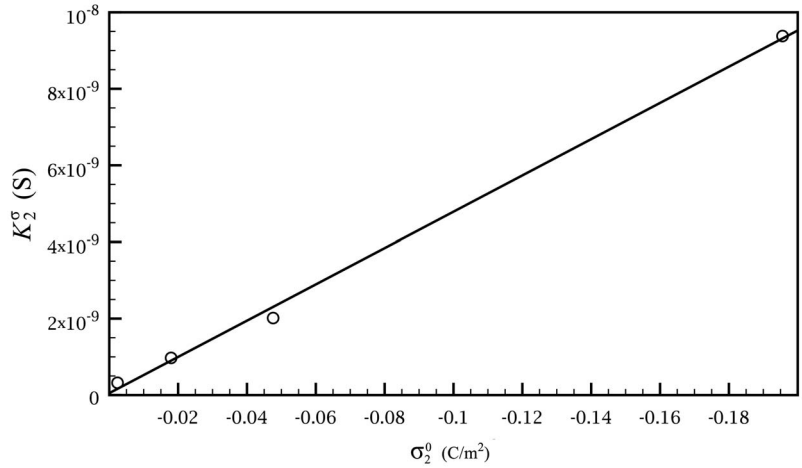

Figure 4. Correlation between surface conductivity (calculated with $l = b = 0.15$ μm) and independently measured surface charge density. The line is a linear regression through the experimental points.

https://doi.org/10.1346/CCMN.2018.064087 Published online by Cambridge University Press

this information, equations 6 and 7 can be solved for $y^{ek} = F\zeta/RT$. Table 1 summarizes the various double layer parameters obtained in this manner.

DISCUSSION

Inspection of Table 1 shows that the diffuse-layer surface conductivity contributions of each electrolyte are independent of electrolyte concentration and are about 0.1 nS. The part of the surface conductivity that originates in the inner part of the double layer is roughly the same order of magnitude (or somewhat lower) at a 1 mM concentration and linearly increases with increased concentration to reach values that are 10–60 times larger than the diffuse contribution. This indicates that the inner part of the double layer is more and more important at higher electrolyte concentrations. Due to better screening, larger parts of the surface charge density will be compensated closer to the surface, *i.e.* within the inner part of the double layer. In connection with a concentration-independent ionic mobility in the inner double layer (see below), this also implies that the ionic transport in this part of the double layer becomes more important as the electrolyte concentration is increased.

For the ζ potentials, we observed the same order of values as for the diffuse part of the surface conductivity mentioned above: $Li^+ \approx Na^+ > K^+ > Cs^+$, whereas the ζ potentials for divalent counterions were more or less the same for a given concentration (Table 1). Somewhat

Table 1. Dukhin number, surface conductivity, ratio of inner to diffuse layer surface conductivity, and electrokinetic potential of kaolinite suspensions at 25ºC.

c^∞ (mol/m^3)	Du_2	K_2^σ (nS)	$K_2^{\sigma^i}/K_2^{\sigma^d}$	ζ (mV)
LiCl, $K_2^{\sigma^d} = 6.7\pm0.3\cdot10^{-10}$ S, $Du_2^i = 0.33\pm0.02$				
1	1.48	0.9	0.3	−88
5	0.60	1.7	1.6	−57
10	0.41	2.4	2.5	−46
50	0.36	10.4	14.5	−25
NaCl, $K_2^{\sigma^d} = 7.1\pm0.2\cdot10^{-10}$ S, $Du_2^i = 0.23\pm0.01$				
1	1.18	0.9	0.3	−85
5	0.41	1.5	1.4	−54
10	0.35	2.6	2.7	−43
50	0.23	8.8	11.3	−24
KCl, $K_2^{\sigma^d} = 4.1\pm0.2\cdot10^{-10}$ S, $Du_2^i = 0.18\pm0.01$				
1	0.55	0.6	0.5	−55
5	0.26	1.4	2.5	−32
10	0.20	2.2	4.5	−24
50	0.20	10.7	25.3	−12
CsCl, $K_2^{\sigma^d} = 1.4\pm0.1\cdot10^{-10}$ S, $Du_2^i = 0.16\pm0.01$				
1	0.28	0.3	1.3	−25
5	0.17	1	5.9	−13
10	0.17	2.0	13.4	−9
50	0.16	9.4	65.9	−4
$CaCl_2$, $K_2^{\sigma^d} = 5.4\pm0.4\cdot10^{-10}$ S, $Du_2^i = 0.20\pm0.01$				
1	0.50	0.9	0.7	−38
5	0.28	2.5	3.6	−23
10	0.24	4.3	6.9	−18
50	0.19	16.9	30.4	−10
$SrCl_2$, $K_2^{\sigma^d} = 6.1\pm0.6\cdot10^{-10}$ S, $Du_2^i = 0.21\pm0.02$				
1	0.55	1	0.6	−41
5	0.27	2.4	2.9	−25
10	0.27	4.9	7.0	−20
50	0.20	17.8	28.2	−11
$BaCl_2$, $K_2^{\sigma^d} = 4.8\pm0.5\cdot10^{-10}$ S, $Du_2^i = 0.20\pm0.01$				
1	0.45	0.9	0.8	−35
5	0.28	2.6	4.5	−21
10	0.23	4.5	8.2	−16
50	0.19	18	36.3	−9

https://doi.org/10.1346/CCMN.2018.064087 Published online by Cambridge University Press

surprising was the fact that Cs^+ was more effective in lowering the ζ potential than divalent counterions. This, however, was not due to a very high inner-layer affinity, but it was rather due to the low $K_2^{\sigma^d}$ value that caused the large $K_2^{\sigma^i}/K_2^{\sigma^d}$ values, which are in line with the substantial inner-layer Cs^+ mobility calculated above. Although a mobility ratio of around 0.6 may hint towards a certain specificity in the inner part of the double layer, this value can equally be rationalized by considering that the surfaces may be quite rough so that the ions have to follow a tortuous path (Lyklema, 2001) or that the estimated characteristic length is somewhat off. However, on the basis of the current data set it is rather difficult to reach a final conclusion.

A qualitative picture on where the observed ion specificity originates, *i.e.* in the diffuse part or in the inner part of the double layer, can be developed if the ionic mobilities of all the counterions are known. This would permit the charge density in the inner part of the double layer to be calculated *via* equation 1 and thus allow a comparison between the different counterions.

In the following text, a simple way to estimate the order of magnitude of the mobility ratio u_2^i/u_2^∞ will be presented. The general idea for this approach comes from Verbich *et al.* (1999). These authors developed a clever method to estimate mobility ratios by exploiting the varying Stern layer adsorbability of different counterions on the same surface. In short, they observed that different counterions influence isoconductive points ($K^*/K^L = 1$) quite substantially. Furthermore, they noticed that the Dukhin number at the isoconductive point (icp) is only determined by the ion diffusion coefficients and the particle geometry. Having identified one counterion that does not adsorb in the inner part of the double layer and a counterion that does adsorb, they compared the Dukhin numbers at the icp's to derive:

$$\frac{u_i^i}{u_i^\infty} \approx \frac{(1+3m_j/z_j^2)\cdot z_i \cdot c^\infty(\mathrm{icp})_i}{c^\infty(\mathrm{icp})_j} \tag{8}$$

where i indicates the counterion that specifically adsorbs, j is the counterion that does not specifically adsorb, and $c^\infty\ (\mathrm{icp})_{i,j}$ denotes the concentrations at the icp. It must be noted that in their derivation the authors assumed that the surface charge density does not vary with electrolyte concentration or type. For this reason and because no counterion can be identified that does not adsorb in the inner part of the double layer (*cf.* Table 1), equation 8 cannot be used to estimate inner layer mobilities in the systems investigated in the present study.

In the present case, the Du_2^i constancy essentially permitted an estimate of the order of magnitude of the counterion mobility in the inner part of the double layer. As remarked above, the Dukhin number at the icp ($Du_{2,\mathrm{icp}}$) is fully determined by the particle shape and the ion diffusion coefficients. The Dukhin number at the icp is, thus, a quantity that can be calculated using equation 2 by setting $K^*/K^L = 1$. Combined with the observation that Du_2^i is constant and counterion-specific, extracting some information about the ionic mobility in the inner part of the double layer by comparing Du_2^i and the Dukhin number values at the icp should be possible. Expressing Du_2 in terms of charge densities and ionic mobilities (see Weber and Stanjek, 2017, for a summary of the relevant equations and references),

$$Du_2 = \frac{1}{K_2^L l} u_2^\infty \sigma_2^d \left(1+\frac{3m_2}{z_2^2}\right)\cdot\left(1+\frac{K_2^{\sigma^i}}{K_2^{\sigma^d}}\right) \tag{9}$$

and dividing by

$$Du_2^i = \frac{1}{K_2^L l} u_2^i \sigma_2^i \tag{10}$$

provides for a given counterion at a given concentration.

$$\frac{Du_2}{Du_2^i} = \left(1+\frac{3m_2}{z_2^2}\right)\cdot\frac{\sigma_2^d u_2^\infty}{\sigma_2^i u_2^i} + 1 \tag{11}$$

Equation 11 is not very useful, because the ionic mobility in the inner part of the double layer occurs in the equation as a product term with the inner layer charge density. This quantity can only be determined if the surface and diffuse layer charge densities are simultaneously available ($\sigma^i = -\sigma^0 - \sigma^d$). The σ^i values are available for a K-kaolinite, a Ba-kaolinite (Weber and Stanjek, 2017), and for the Cs sample studied here. These experimental results suggest that $\sigma_2^d/\sigma_2^i \approx 1$ at the icp for monovalent counterions. This means that under these conditions the surface charge density is equally compensated in the diffuse and inner parts of the double layer. Accepting this approximation for the moment and restricting equation 11 to the isoconductive point, it can be reorganized as follows:

$$\frac{u_2^i}{u_2^\infty} \approx \frac{\left(1+\frac{3m_2}{z_2^2}\right)}{(Du_{2,\mathrm{icp}}/Du_{2,\mathrm{icp}}^i)-1} \tag{12}$$

and equation 12 provides $\frac{u_{Cs}^i}{u_{Cs}^\infty} \approx 0.74 \pm 0.05$ for the Cs^+ mobility ratio, which compares reasonably well with the 0.6 ± 0.03 ratio determined above. For the K-kaolinite, Weber and Stanjek (2017) determined $\frac{u_K^i}{u_K^\infty} \approx 1.06 \pm 0.04$, which agrees well with the ≈ 1.05 value obtained from equation 12. Proceeding in the same manner for the other counterions gives: $u^i/u^\infty \approx 0.76 \pm 0.07$ for Li^+, $\approx 0.75 \pm 0.07$ for Na^+, and $\approx 0.88 \pm 0.07$ for K^+.

For divalent counterions, the situation is somewhat different. For the Ba-kaolinite studied in Weber and Stanjek (2017), the mobility ratio determined from the correlation between surface conductance and surface charge density was $u_{Ba}^i/u_{Ba}^\infty \approx 0.54 \pm 0.02$, whereas the mobility determined from equation 12 was $u_{Ba}^i/u_{Ba}^\infty \approx 0.8 \pm 0.1$. This might be due to the steeper surface-

https://doi.org/10.1346/CCMN.2018.064087 Published online by Cambridge University Press

charge density increase with increased divalent counterion concentrations. As a result, the σ_2^d/σ_2^i ratio may be <1 or at least less than the monovalent counterion ratio and as a consequence, the mobility ratio will be somewhat overestimated. For the divalent counterions studied here, equation 12 delivers: $u^i_{Ca}/u^\infty_{Ca} \approx 0.65 \pm 0.06$, $u^i_{Ba}/u^\infty_{Ba} \approx 0.73 \pm 0.08$, and $u^i_{Sr}/u^\infty_{Sr} \approx 0.68 \pm 0.08$.

Because very few complete data sets were available, judging the accuracy of the approximation used to arrive at equation 12 was very difficult. Therefore, absolute values of the mobility ratios will not be discussed in detail, but rather note that the order of magnitude of the values are very reasonable in comparison to experimental literature values for a large variety of surfaces (Rowlands and O'Brien, 1995; Rasmussen *et al.*, 1997; Lyklema and Minor, 1998; Minor *et al.*, 1998a, 1998b; Löbbus *et al.*, 2000; Lyklema, 2001, 2002, 2003; Djerdjev *et al.*, 2003; Jiménez *et al.*, 2005). The main point is that counterion mobilities in the inner part of the double layer are substantial, which is an observation that will be beneficial for constraining the parameters in SIP modeling.

No obvious trends were noted when the mobility ratios of different counterions of the same charge were compared. The invariance of ionic mobility with respect to counterion nature argues against a chemically driven mechanism (*i.e.* any kind of force that acts on the counterions in addition to purely electrostatic attraction) that causes the observed specificity. Figure 5 illustrates that the apparent specificities are related to the counterion volumes. On the left side of Figure 5, the inner layer charge density was estimated using equation 1 and plotted as a function of counterion volume. The right side of Figure 5 shows the corresponding plot for the diffuse layer charge density. The ionic radii were obtained from Marcus (1988) and were converted into ion volumes by assuming a spherical symmetry.

The charge density of the inner layer decreases as monovalent counterion size increases and reaches a constant value for K^+ and Cs^+. In comparison to the inner layer, the charge density of the diffuse layer shows a more pronounced dependence on counterion volume for monovalent ions. Similar trends can of course be observed for the ζ -potentials and the surface conductivities of the diffuse layer. For the divalent counterions, trends were not evident for the inner layer or for the diffuse layer charge densities. In principle, this result is in line with the literature for other systems. Kruyt and Klompé (1943), for instance, observed a similar condition when the critical coagulation concentrations of AgI sols were compared. Breeuwsma and Lyklema (1971) observed pronounced ion specific effects on the surface charge density of monovalent cations adsorbed to hematite. In contrast to the monovalent ions, no ion specificity was observed for Ca^{2+}, Ba^{2+}, and Sr^{2+}. Although ion specific effects have sometimes been observed for divalent cations (Dove and Craven, 2005), the effects were not as pronounced in comparison to monovalent cations. As suggested by Lyklema (2003), the effect of doubling the charge (in going from monovalent to divalent counterion) possibly dominates the more subtle influence of ion size.

The dependencies found for monovalent counterions indicate that the apparent differences are less due to a chemical specificity, but are rather related to the counterion volume. In the case of the inner layer, it may be reasoned that the available surface space permits more Li and Na to accumulate in comparison to the larger K and Cs. For the diffuse layer, the situation is somewhat more involved. The theory of O'Brien and Ward (1988) is based on the Poisson-Boltzmann (PB) theory, which assumes that the ions have no volume. The observed trends may at least be in part a result of neglecting ion volumes. Although corrections to the PB theory, which take ion volume into account, are available (*e.g.* Bikerman, 1942; Biesheveul and van Soestbergen, 2007; López-García and Horno, 2011), comparatively little has been done to include the finite volume of ions into electrokinetic theories (Aranda-Rascón *et al.*, 2009a, 2009b). On top of the lack of a suitable theory for non-spherical particles, the different behavior of divalent ions indicates a more complicated

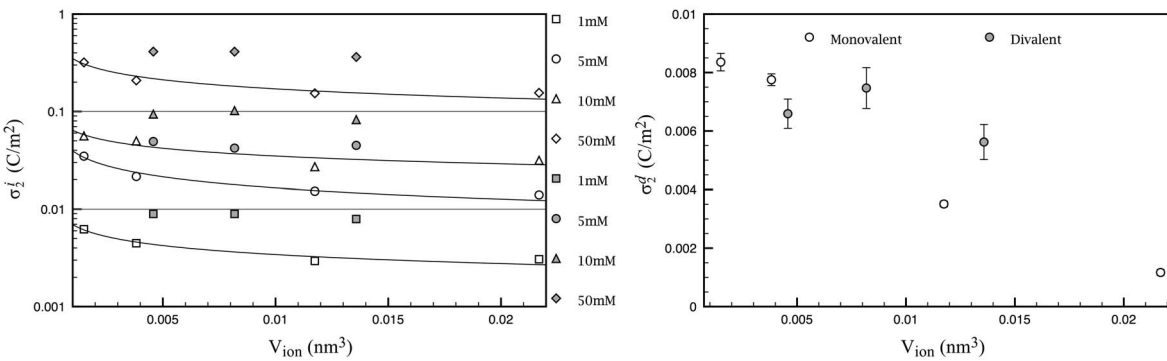

Figure 5. Estimated inner-layer charge density and diffuse layer charge density of counterions as a function of counterion volume. Lines are shown to guide the eye. Open symbols indicate monovalent counterions and filled symbols divalent counterions.

https://doi.org/10.1346/CCMN.2018.064087 Published online by Cambridge University Press

situation. Realizing that the ion specific effects observed in double layer parameters may be at least in part an effect of the finite ion size may be useful in modeling studies, where ion-specific effects are usually treated in a chemical sense within the inner double layer.

CONCLUSION

By studying the low-frequency electrical conductivity of clay suspensions, a number of useful double layer parameters can be derived. In general, the surface conductance was shown to be substantial for kaolinite particles and that only a fraction of it originates at the shear plane, which indicates that a major part of counterion adsorption occurs in the inner part of the electrical double layer. The inner part of the electrical double layer becomes more and more important at higher electrolyte concentrations.

The ionic mobilities of counterions within the inner part of the double layer were estimated by studying the isoconductive points and showed that all studied counterions have a substantial mobility in the inner part of the double layer. Although we cannot say much about the accuracy of the approximations used to derive equation 12, the cases where independent data were available showed good agreement for monovalent ions. Some caution should be exercised with multivalent counterions, where less agreement was found with independent data.

With respect to different counterions, the conclusion is that monovalent counterions behave distinctly differently from divalent counterions. While monovalent counterions showed pronounced differences in double layer parameters, the divalent counterions basically behaved alike. Ion-specific effects of monovalent counterions are most readily observed in the diffuse part of the double layer *via* ζ-potentials and related quantities. Both the estimated charge density of the inner layer and the diffuse layer charge density showed trends with counterion volume for monovalent counterions. Hopefully, the findings of this study, especially those regarding ionic mobilities in the Stern layer, will help to constrain parameters in the modeling of SIP spectra and to improve the understanding of these very complex systems.

Future work should include the study of pure clay minerals and defined mixtures of clay minerals. By performing such experiments, the impact of accompanying phases on electro-surface parameters may possibly be estimated. Studying mixtures of materials with low and high cation exchange capacities would be particularly interesting.

ACKNOWLEDGMENTS

The authors thank Christian Detellier for his competent and friendly handling of the review process. The efforts of two anonymous reviewers, who provided helpful comments, are appreciated.

REFERENCES

Aranda-Rasćon, M.J., Grosse, C., López-García, J.J., and Horno, J. (2009a) Electrokinetics of suspended charged particles taking into account the excluded volume effect. *Journal of Colloid and Interface Science*, **335**, 250–256.

Aranda-Rasćon, M.J., Grosse, C., López-García, J.J., and Horno, J. (2009b) Influence of the finite ion size on the predictions of the standard electrokinetic model: Frequency response. *Journal of Colloid and Interface Science*, **366**, 857–864.

Biesheveul, P.M. and van Soestbergen, M. (2007) Counterion volume effects in mixed electrical double layers. *Journal of Colloid and Interface Science*, **316**, 490–499.

Bikerman, J.J. (1942) XXXIX. Structure and capacity of electrical double layer. *The London, Edinburgh, and Dublin Philosophical Magazine and Journal of Science*, **33**, 384–397.

Breeuwsma, A. and Lyklema, J. (1971) Interfacial electrochemistry of hematite (α-Fe_2O_3). *Discussions of the Faraday Society*, **52**, 324–333.

Brunauer, S., Emmett, P.H., and Teller, E. (1938) Adsorption of gases in multimolecular layers. *Journal of the American Chemical Society*, **60**: 309–319.

Chassagne, C., Mietta, F., and Winterwerp J.C. (2009) Electrokinetic study of kaolinite suspensions. *Journal of Colloid and Interface Science*, **336**, 352–359.

Delgado, A.V., Gonzalez-Caballero, F., Hunter, R.J., Koopal, L.K., and Lyklema, J. (2007) Measurement and interpretation of electrokinetic phenomena. *Journal of Colloid and Interface Science*, **209**, 194–224.

Djerdjev, A.M., Beattie, J.K., and Hunter, R.J. (2003) An electroacoustic and high-frequency dielectric response study of stagnant layer conduction in emulsion systems. *Journal of Colloid and Interface Science*, **265**, 56–64.

Dove, M. and Craven, C.M. (2005) Surface charge density on silica in alkali and alkaline earth chloride electrolyte solutions. *Geochimica et Cosmochimica Acta*, **69**, 4963–4970.

Dzenitis, J.M. (1997) Soil chemistry effects and flow prediction in electroremediation of soil. *Environmental Science & Technology*, **31**, 1191–1197.

Jennings, B.R. and Parslow, K. (1988) Particle size measurement: The equivalent spherical diameter. *Proceedings of the Royal Society of London A: Physical, Mathematical and Engineering Sciences*, **419**, 137–149.

Jiménez, M.L., Arroyo, F.J., Carrique, U., Kaatze, F., and Delgado, A.V. (2005) Determination of stagnant layer conductivity in polystyrene suspensions: Temperature effects. *Journal of Colloid and Interface Science*, **281**, 503–509.

Kruschwitz, S., Binley, A., Lesmes, D., and Elshenawy, A. (2010) Textural controls on low frequency electrical spectra of porous media. *Geophysics*, **75**, 113–123.

Kruschwitz, S., Carsten Prinz, C., and Zimathies, A. (2016) Study into the correlation of dominant pore throat size and SIP relaxation frequency. *Journal of Applied Geophysics*, **135**, 375–386.

Kruyt, H.R. and Klompé, M.A.M. (1943) Solkonzentration und Flockung beim AgJ-sol. *Kolloid-Beihefte*, **54**, 484–553.

Labbez, C., Fievet, P., Szymczyk, A., Simon, C., Vidonne, A., Foissy, A., and Pagetti, J. (2001) Hydraulic resistance measurements combined with electrical or diffusional resistance measurements for determination of pore size in MF membranes. *Desalination*, **141**, 291–299.

Löbbus, M., van Leeuwen, H., and Lyklema, J. (2000) Streaming potentials and conductivities of latex plugs: Influence of the valency of the counterion. *Colloids and Surfaces A: Physicochemical and Engineering Aspects*, **161**, 103–113.

Lopez-García, J.J. and Horno, J. (2011) Poisson-Boltzmann description of electrical double layer including ion size effects. *Langmuir*, **27**, 13970–13974.

Lyklema, J. (1995) Electrokinetics and related phenomena. Chapter 4, pp. 4.1–4.135 in: *Fundamentals of Interface and Colloid Science* (J. Lyklema, editor) Volume II, Elsevier.

Lyklema, J. (2001) Surface conduction. *Journal of Physics: Condensed Matter*, **13**, 5027–5034.

Lyklema, J. (2002) Specificity in the statics and dynamics of surface-confined ions. *Molecular Physics*, **100**, 3177–3185.

Lyklema, J. (2003) Lyotropic sequences in colloid stability revisited. *Advances in Colloid and Interface Science*, **100–102**, 1–12.

Lyklema, J. and Minor, M. (1998) On surface conduction and its role in electrokinetics. *Colloids and Surfaces A: Physicochemical and Engineering Aspects*, **140**, 33–41.

Marcus, Y. (1988) Ionic radii in aqueous solutions. *Chemical Reviews*, **88**, 1475–1498.

Minor, M., van Leeuwen, H.P., and Lyklema, J. (1998a) Low-frequency dielectric response of polystyrene latex dispersions. *Journal of Colloid and Interface Science*, **206**, 397–406.

Minor, M., van der Linde, A.J., and Lyklema, J. (1998b) Streaming potentials and conductivities of latex plugs in indifferent electrolytes. *Journal of Colloid and Interface Science*, **203**, 177–188.

O'Brien, R.W. and Rowlands, W.N. (1993) Measuring the surface conductance of kaolinite particles. *Journal of Colloid and Interface Science*, **159**, 471–476.

O'Brien, R.W. and Ward, D.N. (1988) The electrophoresis of a spheroid with a thin double layer. *Journal of Colloid and Interface Science*, **121**, 402–413.

Rasmussen, M., Rowlands, W.N., O'Brien, R.W., and Hunter, R.J. (1997) The dynamic mobility and dielectric response of sodium bentonite. *Journal of Colloid and Interface Science*, **189**, 92–100.

Revil. A. (2012) Spectral induced polarization of shaly sands: Influence of the electrical double layer. *Water Resources Research*, **48**, 1–23.

Revil, A. (2014) Discussion Comment on: "On the relationship between induced polarization and surface conductivity: Implications for petrophysical interpretation of electrical measurements". *Geophysics*, **79**, X1–X10.

Revil, A. and Florsch, N. (2010) Determination of permeability from spectral induced polarization in granular media. *Geophysical Journal International*, **181**, 1480–1498.

Rouquerol, J., Avnir, D., Fairbridge, D.H., Everett, C., Haynes, J.H., Pernicone, N., Ramsay, J.D.F., Sing, K.S.W., and Unger, K.K. (1994) Recommendations for the characterization of porous solids. *Pure and Applied Chemistry*, **66**, 1739–1758.

Rowlands, W.N. and O'Brien, R.W. (1995) The dynamic mobility and dielectric response of kaolinite particles. *Journal of Colloid and Interface Science*, **175**, 190–200.

Scott, J.B.T. and Barker, R.D. (2005) Characterization of sandstone by electrical spectroscopy for stratigraphical and hydrogeological investigations. *Quarterly Journal of Engineering and Geology and Hydrogeology*, **38**, 143–154.

Slepetys, R.A. and Cleland, A.J. (1993) Determination of shape of kaolin pigment particles. *Clay Minerals*, **28**, 495–508.

Tarasov, A. and Titov, K. (2007) Relaxation time distribution from time domain induced polarization measurements. *Geophysical Journal International*, **170**, 31–43.

Verbich, S.V., Dukhin, S.S., and Matsumura, H. (1999). Investigation of dynamic stern layer of liposomes by measurements of conductivity and electrophoresis. *Journal of Dispersion Science and Technology*, **20**, 83–104.

Weber, C. and Stanjek, H. (2017) Low-frequency electric conductivity of aqueous kaolinite suspensions: Surface conductance, electrokinetic potentials and counterion mobility. *Clay Minerals*, **52**, 299–313.

Weber, C., Heuser, M., Mertens, G., and Stanjek, H. (2014) Determination of clay mineral aspect ratios from conductometric titrations. *Clay Minerals*, **49**, 17–26.

Weller, A. and Slater, L. (2015) Induced polarization dependence on pore space geometry: Empirical observations and mechanistic predictions. *Journal of Applied Geophysics*, **123**, 310–315.

Weller, A., Slater, L., and Nordsiek, S. (2013) On the relationship between induced polarization and surface conductivity: Implications for petrophysical interpretation of electrical measurements. *Geophysics*, **78**, D315–D325.

Weller, A., Zhang, Z., and Slater, L. (2015) High-salinity polarization of sandstones. *Geophysics*, **80**, D309–D318.

Weller, A., Zhang, Z., Slater, L., Kruschwitz, S., and Halisch, M. (2016) Induced polarization and pore radius – A discussion. *Geophysics*, **81**, D519–D526.

(*Received 13 October 2017; revised 12 February 2018; Ms. 1218; AE: C. Detellier*)